

Algorithm of emissivity spectrum and temperature separation based on TASI data

YANG Hang^{1,2}, ZHANG Lifu¹, ZHANG Xuewen^{1,2}, FANG Conghui³, TONG Qingxi¹

1. The State Key Laboratory of Remote Sensing Sciences, Institute of Remote Sensing Applications, Chinese Academy of Sciences, Beijing 100101, China;

2. Graduate University of Chinese Academy of Science, Beijing 100039, China;

3. School of the Earth Sciences and Resources, China University of Geosciences, Beijing 100083, China

Abstract: The retrieval and application of emissivity spectrum and temperature are key issues in thermal infrared remote sensing. Thermal airborne hyperspectral imager has 32 bands from 8 μm to 11.5 μm , which can provide abundant useful information for the retrieval of emissivity spectrum and temperature. This paper establishes regression between MMD and β min using 274 laboratory reflectance and field emissivity spectra, analyzes its accuracy using the data field measuring, and evaluates urban surface diurnal temperature range. The result shows that: (1) the average absolute difference between the temperature of retrieval and the measurement is 1.8 K, and the relative difference is 0.59%; (2) the mean difference between the broadband emissivity and the mean emissivity from TASI is 0.036, and the standard error of difference is 0.032. Because of the effects of scale and atmosphere, the predicted value does not equal to the laboratory measurement, but the pattern of predicts is similar to the laboratory measurement; (3) the result of diurnal temperature range is reasonable. Therefore, the accuracy of this method can satisfy operational application and it is feasible to retrieve the emissivity spectrum and temperature for TASI data.

Key words: thermal infrared airborne hyperspectral data, temperature, emissivity spectrum, diurnal temperature range, TES

CLC number: TP701 **Document code:** A

Citation format: Yang H, Zhang L F, Zhang X W, Fang C H and Tong Q X. 2011. Algorithm of emissivity spectrum and temperature separation based on TASI data. *Journal of Remote Sensing*, 15(6): 1242–1254

1 INTRODUCTION

Although imaging spectral technique is a powerful tool in collection, analysis, and modeling of environmental data, the application and study on thermal infrared remote sensing are not well developed. With the development of remote sensing, more and more satellites with single or multispectral sensors were launched, and more attention was paid to thermal infrared data. The emissivity and temperature retrieved from thermal infrared data will have an extremely important significance for scientific research and operational application. Surface emissivity is an important parameter, and emissivity spectra are often used to distinguish objective and interpret features. Land surface temperature is an important parameter for understanding land surface processes. Through measurement of surface temperatures as related to specific landscape and biophysical components and then through relating surface temperatures with energy fluxes for specific landscape phenomena or processes (sobrino,

et al., 2006). Therefore, temperature and emissivity separation are the key variables of infrared remote sensing. However, because the algorithms of temperature and emissivity separation from thermal infrared data involves solving $N+1$ parameters with N equations, one has to assume or educe a new empirical formulation so as to make the equation complete. Generally, most algorithms vary with different assumption of emissivity. Presently, many methods are essentially successfully developed for multi-spectral thermal sensors, including the reference channel method (REF) (Kahle, *et al.*, 1980), Normalized emissivity method (NEM) (Gillespie, 1985), Alpha-derived emissivity (ADE) (Kealy & Gabell, 1990), the maximum and minimum difference method (Matsunaga, 1992), iterative spectral smooth temperature and emissivity separation (ISSTES) (Borel, 1998), and TES method (Gillespie, *et al.*, 1998). Among those methods, TES method is composed by three modules: NEM, RAT, and MMD. It is proved that the emissivity error is within ± 0.015 using the Aster simulated data (Yang, *et al.*, 2010). The TES method

Received: 2010-11-03; **Accepted:** 2011-05-06

Foundation: The National High Technology Research and Development Program of China (No. 2008AA121103, 2008AA121102) and the National Natural Science Foundation of China (No. 41072248)

First author biography: YANG Hang (1979—), male, Ph. D. candidate, majors in theoretical and applied research on hyperspectral remote sensing. E-mail: yanghang1979@126.com

Corresponding author biography: ZHANG Lifu (1967—), male, professor, his research interests are the theory and application of hyperspectral remote sensing. E-mail: zhanglf@irsa.ac.cn

was used to the thermal infrared multispectral data in HAPEX-Sahel with an error of about 3 K. (Schmugge, *et al.* 1998)

However, previous studies mainly focus on the single and multispectral thermal infrared data. With the development of sensor-hardware technology, hyperspectral thermal infrared data has created favorable conditions for studying on land surface emissivity and temperature. High resolution spectra includes fine surface emissivity characteristics, and aids to form more steady constraint conditions and improves the retrieval accuracy. Thermal Airborne Hyperspectral Imager (hereinafter referred to as the TASI) is one of the most advanced airborne thermal infrared imagers, which has 32 bands in the thermal infrared region (8—11.5 μm) of the electromagnetic spectrum, with wavelength spacing of 0.1095 μm , FWHM (Full width at half maximum) of 0.0548 μm , and total fields of view of 40°. Fig. 1 is the sensitivity of each TASI channel to radiance. This work is to build a new empirical module based on the TASI band setting, use the TES algorithm to TASI data, and validate the reliability of the algorithm. On that basis, we further study and analyze the characteristics of surface temperature and emissivity, and then discuss the probability of identification using emissivity spectra.

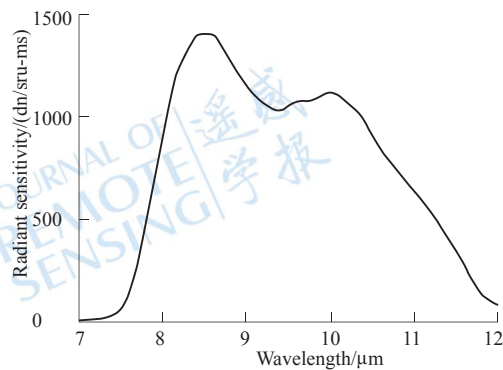


Fig. 1 The sensitivity of TASI each channel to radiance

2 DATA SOURCE

The experiment data is important to validate and test the algorithms developed for temperature and emissivity separation using the thermal airborne hyperspectral imager. The aircraft images and the in situ data were acquired simultaneously in the framework of field campaigns at Shijiazhuang, Hebei province in 2010. The fly region lies in 38°0'10"N–38°6'20"N, 114°26'34.01"E–114°30'0.01"E, with 30 km in north-south, and 5.03 km in east-west, covering an area of 57.34 km². The aircraft campaign was conducted from 2010-07-25–2010-08-15, and three time phase (morning, noon, evening), two heights (0.5 km and 1 km) images of TASI were acquired. The particular flight scheme is listed in Table 1. Vertical earth observation reduces angle effect for each image. Fig. 2 is the color image of study area.

Table 1 The time and height of airborne campaign

Time	Height/km
Noon, 2010-07-25	0.5
Evening, 2010-07-25	0.5
Evening, 2010-07-27	1.0
Morning, 2010-07-29	0.5
Morning, 2010-08-07	1.0
Noon, 2010-08-15	1.0



Fig. 2 The color map of selected study area

In the field campaign, the typical surface temperature and emissivity were measured in step with the airborne campaign. The temperature measurement time was within 5 min before or after the covering time for plane. For each sample pixel, about 20–30 temperature values were read uniformly, whose average was calculated to represent the true temperature for the sample pixel, and the longitude-latitude coordinates were also recorded. Temperature measurements were conducted using different broadband and multiband field thermal radiometers. MINOLTA/LAND infrared thermometer will response to broadband radiometers, while model CIMEL CE312 is multiband radiometer. The accuracy of the two instruments is about 0.1 K. Field measurements include road (cement and asphaltum), crop (maze, pachyrhizus and peanut), building roof, water, and plaza *etc.*. These measured data were used to precision analysis of temperature and emissivity separation.

3 DATA PROCESSING

3.1 Data calibration

(1) Radiometric Calibration of TASI data

To acquire the objective radiance, radiance calibration of every band is essential before measuring the objective radiance, indicating that the digital number values (*DN*) recorded by the thermal infrared imaging spectrometer must be translated spectral radiance values. The radiance calibration method of TASI data is based on the assumption of a linear sensor response function, and is implemented by the means of measuring two known temperature and emissivity of standard blackbody. Firstly, it is assumed that the digital number values the TASI recorded have linear relationship with the radiance, and then radiance calibration band by band can be calculated as:

$$L = c_1 \times DN + c_2 \quad (1)$$

where c_1 and c_2 are gain and offset of instrument spectral response function. This procedure can be implemented automatically by the TASI data procession software.

(2) Calibration of Infrared thermometer

Compared with common water thermometer, infrared thermometer has the defect of weak stability and is easily to attenu-

ation. In order to acquire the accurate temperature, thermometer calibration is a requisite before and after field experiment. The thermometer calibration procedure uses cooling pure water in lieu of low temperature blackbody and hot pure water in lieu of high temperature blackbody. Generally, temperature of cooling pure water is the same as the environmental temperature, and temperature of hot pure water is above 45°C. It is considered that water temperature should be stable and homogeneous when measuring, and the field of view should be full of water. One should make records of the water temperature measured by infrared thermometer and common thermometer separately. When calibrating, cooling water temperature measured by common thermometer is regarded as true temperature, and denoted as $T_{1,true}$; cooling water temperature measured by infrared thermometer is denoted as $T_{1,R}$; hot water temperature measured by common thermometer is denoted as $T_{2,true}$; hot water temperature measured by infrared thermometer is denoted as $T_{2,R}$. There is linear relationship between radiant temperature and true temperature:

$$T_{true} = k_1 \times T_R + k_2 \quad (2)$$

In order to implement radiance temperature calibration one by one, $T_{1,true}$, $T_{1,R}$, $T_{2,true}$ and $T_{2,R}$ were substituted into Eq. (2), and then the coefficients k_1 and k_2 were calculated.

3.2 Atmospheric correction

Atmospheric correction transforms radiance acquired by sensors into ground-leaving radiance. Assuming the land surface is Lambertian, and combining with Kirchhoff law, surface radiance acquired by TASI sensor can be expressed by the following formulation:

$$L_i = \tau_i \varepsilon_i B_i(T_s) + \tau_i (1 - \varepsilon_i) L_{atm\downarrow,i} + L_{atm\uparrow,i} \quad (3)$$

where L_i is radiance of channel i measured by TASI sensor; ε_i is surface emissivity of channel i ; $B_i(T_s)$ is the Planck radiance at surface temperature; τ_i is the atmospheric transmittance of channel i ; $L_{atm\uparrow,i}$ is the up-welling path radiance; $L_{atm\downarrow,i}$ is the down-welling sky radiance. According to the studied region, the up-welling path radiance, the down-welling sky radiance, and the atmospheric transmittance consisting with the TASI were obtained by the MODTRAN software. The main preferences were as following:

(1) Model atmosphere selection

In this paper, model atmosphere is Mid-Latitude Summer (45° N); atmospheric path is slant path; vertical water vapor content uses meteorological observation data; CO₂ mixing ratio is 330.0 ppmv; multiple scattering parameter is Distort and number of Distort stream equals to 8; the temperature at first boundary is based on the atmospheric temperature observed simultaneously at near-surface.

(2) Aerosol and cloud option

Aerosol model is set to URBAN extinction, default VIS = 5 km; seasonal aerosol profile (ISEASN) is set to SPRING-SUMMER; the wind speed is set to the value measured simultaneously at near-surface; the weather is fine, and there is no cloud or rain. Fig. 3 is the up-welling path radiance and down-welling sky radiance consisting with the TASI by the MODTRAN software. Fig. 4 is the atmospheric spectral transmittance.

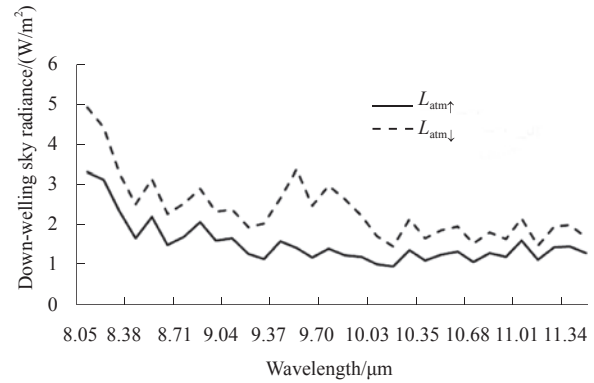


Fig. 3 The up-welling path radiance and down-welling sky radiance by the MODTRAN software for TASI data

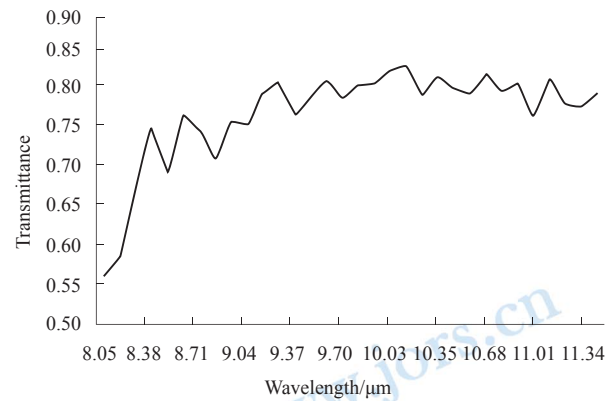


Fig. 4 The atmospheric transmittance by the MODTRAN software for TASI data

On the premise that the optimal objective temperature could be estimated, the objective emissivity can be calculated by the following equation:

$$\varepsilon_i = \frac{L_{gi} - L_{atm\downarrow,i}}{B_i(T_s) - L_{atm\downarrow,i}} \quad (4)$$

where $L_{gi} = (L_i - L_{atm\uparrow,i}) / \tau_i$.

4 METHOD FOR TEMPERATURE AND EMISSIVITY SEPARATION

4.1 The algorithm of temperature and emissivity separation

Aster team developed a new algorithm of temperature and emissivity separation (Gillespie, *et al.*, 1998). The TES method is composed by three basic modules: NEM, Ratio, MMD.

NEM module (normalized emissivity method): firstly the emissivity of each channel is assumed to be 0.97, in order to calculate a temperature and the other emissivities. These emissivities permit iterative correction for removing the effect of down-welling sky irradiance, and then an initial surface temperature T_s^0 can be estimated.

Ratio module: the relative spectral would be calculated by the Eq. (5). An important advantage of the method is that the emissivity spectral shape would be kept during the process of iteration.

$$\beta_i = \frac{\varepsilon_i}{\varepsilon} = \frac{L_i / B_i(T_s^0)}{\left(\frac{1}{N} \sum_{i=1}^N L_i\right) / \left(\frac{1}{N} \sum_{i=1}^N B_i(T_s^0)\right)} \quad (5)$$

where, L_i is the radiance of channel i after atmospheric correction; T_s^0 is the initial temperature calculated by the NEM module; ε_i is surface emissivity of channel i ; $\bar{\varepsilon}$ is the average emissivity; N is the number of bands, for TASI data, $N=32$.

MMD module: the empirical relationship between ε_{\min} and MMD, where $\text{MMD} = \max(\beta) - \min(\beta)$ is a key feature of the TES algorithm. The ε_{\min} is calculated by the empirical relationship (Eq. (6)).

$$\varepsilon_{\min} = a - b \times \text{MMD}^c \quad (6)$$

where a , b , and c is the coefficients which depend on the analysis of laboratory emissivity spectra, and vary with different sensors. In order to raising the accuracy, it is essential to build a new empirical relationship based on the TASI band setting.

4.2 Surface broadband emissivity (8-12 μm) measurement

Surface broadband emissivity is measured by the portable emissivity apparatus developed and detailed descriptions can be found in Zhang (2009). In this paper, the method can be briefly described as follows:

The measuring principle of this method is the same as that of sealing-cavity method. There are two equations under the conditions of cooling and hot environments:

$$M'_{s1} = \varepsilon_B M'_{B1} + (1 - \varepsilon_B) M'_{E1} \quad (7)$$

$$M'_{s2} = \varepsilon_B M'_{B2} + (1 - \varepsilon_B) M'_{E2} \quad (8)$$

where M'_{s1} is the objective radiance exitance under the condition of cool environment; M'_{s2} is the objective radiance exitance under the condition of hot environment; M'_{B1} is the objective radiance under the condition of cool environment; M'_{B2} is the objective radiance under the condition of hot environment; M'_{E1} is the atmospheric down-welling irradiance; M'_{E2} is irradiance within cavity; ε_B is the objective emissivity. Among all the parameters, M'_{s1} , M'_{s2} , M'_{E1} , and M'_{E2} can be measured directly, and $M'_{B1} = M'_{B2}$. There are hence two unknown numbers. On the basis of Stefan-Boltzman law, the emissivity can be calculated by the following equation:

$$\varepsilon = 1 - \frac{M'_{s1} - M'_{s2}}{M'_{E1} - M'_{E2}} = 1 - \frac{T_{s1}^4 - T_{s2}^4}{T_{E1}^4 - T_{E2}^4} \quad (9)$$

where T_{s1} , T_{s2} , T_{E1} and T_{E2} is the temperature of a black body that would have the same radiance as M'_{s1} , M'_{s2} , M'_{E1} and M'_{E2} , respectively.

4.3 Establishment of the empirical relationship between ε_{\min} and MMD

The empirical relationship between ε_{\min} and MMD was established by analysis of the 274 laboratory reflectance spectra supplied by ASTER and MODIS spectral library, equivalent to emissivity by Kirchhoff's Law. Surface types include water, vegetation, soil, minerals, building materials, and part artificial surface. Based on these data, the empirical relationship consisting with TASI was established. The main steps are as follows:

- (1) These emissivities spectra were resampled into the emissivities consisting with TASI band setting.
- (2) Calculation of ratio by the Eq. (5).
- (3) Calculation of MMD by equation $\text{MMD} = \max(\beta_i) - \min(\beta_i)$ ($i = 1-32$).
- (4) The establishment of the empirical relationship. There is sig-

nificant exponential relationship between ε_{\min} and MMD (Fig. 5):

$$\varepsilon_{\min} = 0.9924 - 0.9174 \times \text{MMD}^{0.9723} \quad (10)$$

($r^2 = 0.988$, $SD = 0.0156$)

The new empirical relationship will replace the original emissivity module of TES algorithm, and then emissivity and temperature will be retrieved using the algorithm from TASI data. Fig. 6 is the temperature image (left) and emissivity image (right) retrieved by this method from TASI image acquired at noon on 2010-08-05.

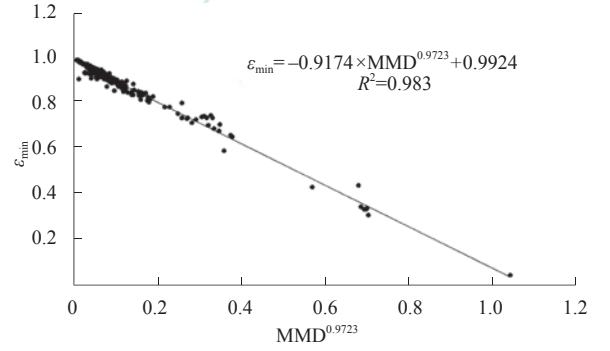


Fig. 5 The exponential relationship between ε_{\min} and MMD

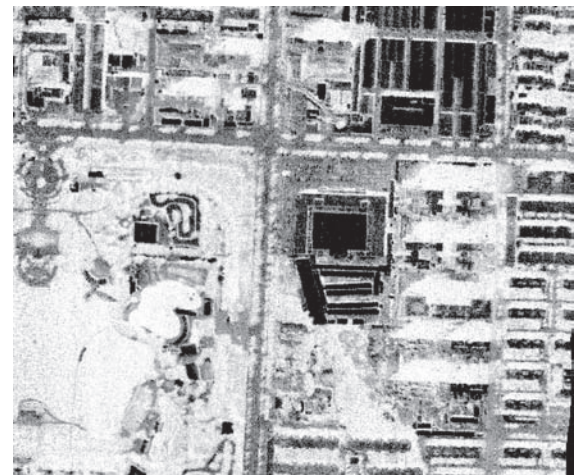


Fig. 6 The image retrieved by this method
(a) temperature; (b) emissivity

5 RESULTS AND ANALYSIS

There are two methods of data resources to evaluate the advantage and disadvantage of algorithms: using both simulated and field data. In this paper, the field data was used to analyze the retrieval accuracy from the two sides of temperature and emissivity.

5.1 Analysis of temperature accuracy

Before the analysis of temperature accuracy, it is necessary to calibrate the infrared temperature into true temperature which is equivalent to be measured by mercury thermometer. The spatial resolution of TASI images is 0.59 m when the flying height is 0.5 km, and the spatial resolution of TASI images is 1.19 m when the flying height is 1 km. Therefore, it is easy to locate the pixel in the TASI image according to the latitude and longitude coordinates recorded during the field campaign, and compare the retrieved temperature with the measured temperature (Table 2).

Table 2 Comparison of retrieved temperature and field-measured temperature for samples

Surface type	True T /K	Retrieve T /K	T deviation /K	Relative deviation/%
Bolin residential roof	302.6	306.4	3.8	1.26
Lianqiang residential roof	304.4	304.7	0.3	0.10
Cement plaza	305.0	306.3	1.3	0.42
Cement road 1	316.2	313.2	3.1	0.97
Cement road 2	304.0	306.4	2.5	0.81
Grass in field	304.0	303.0	1.0	0.34
Maze	295.7	293.8	2.0	0.66
Grass in park	295.8	295.0	0.9	0.29
Granite pavement in park	297.1	296.8	0.3	0.11
Water in park	299.3	298.5	0.9	0.29
River-water	299.2	300.7	1.6	0.52
Black cloth	311.2	307.3	3.9	1.25
White cloth	307.9	305.8	2.1	0.68
mean of T deviation			1.8	0.59
Standard deviation of T deviation			1.2	0.39

As shown in Table 2, the temperature deviations between retrieved and measured temperature vary from 0.3 K to 3.9 K, and the mean of absolute deviation is 1.8 K, and the mean of relative deviation is 0.59%. The Lianqiang residential roof has the highest temperature accuracy, with a deviation is 0.3 K, but the Bolin residential roof has the lowest temperature accuracy. This is because that there are many solar water heaters on the Bolin residential roof, which seriously affects the temperature accuracy, but the Lianqiang residential roof is more homogeneous. Both are cement, the temperature deviation of cement plaza is 1.3 K, while that of cement road is 2.5 K and 3.1 K. This is because that the plaza is broader than road, and the road is seriously affected by the high buildings and tree. The temperature deviation of water in park is 0.9 K, while the value of river water is 1.6 K. The temperature deviation of black cloth is 3.9 K, a little larger, which is possibly because this black cloth is on the slanting river bank with angle effect causing greater influence to temperature accuracy.

5.2 Analysis of emissivity accuracy

In order to analyze the surface emissivity accuracy, the surface narrow-band emissivity of TASI was converted into the surface

broadband emissivity. Table 3 is the comparison of retrieved emissivity and field-measured surface broadband emissivity. The result shows that the mean difference between retrieved and field-measured surface broadband emissivity is 0.036, with the standard deviation of difference of 0.032.

As hyperspectral data of TASI, it is necessary to further analyze the difference between the retrieved emissivity spectrum and the true values. As illustrated in Fig. 7, for main building materials, such as granite, brick, cement, and roof, the retrieved emissivity value is different from the laboratory measured emissivity value, but for the similar surface type, the shapes between the two are similar. The main reason is that the scale of laboratory sample is different from the pixel scale, and the emissivities at the two scales have greater difference. It is important to effectively remove the atmospheric effect for TASI data, and meanwhile considering the sensitivity to surface roughness for laboratory measurement.

Table 3 Comparison of retrieved emissivity and field-measured emissivity

Surface type	True ϵ	Retrieve ϵ	$ \Delta\epsilon $
Black asphalt felt with fine sand	0.948	0.953	0.005
Green asphalt felt with fine sand	0.928	0.882	0.046
Black roofing slate	0.953	0.904	0.049
Red plastic track	0.998	0.917	0.081
Cinder track	0.977	0.930	0.047
Asphalt road	0.912	0.910	0.002
White cement road	0.910	0.917	0.007
Soil	0.959	0.957	0.002
Vegetable	0.981	0.951	0.030
Fake pasture	0.976	0.891	0.086
Mean			0.036
Standard deviation of $ \Delta\epsilon $			0.032

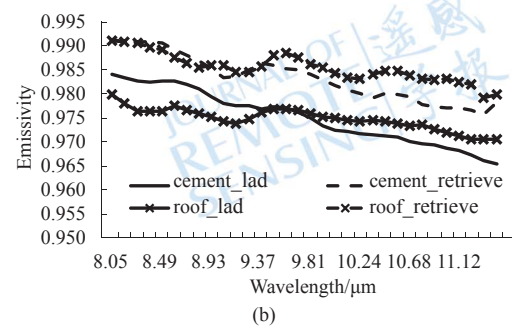
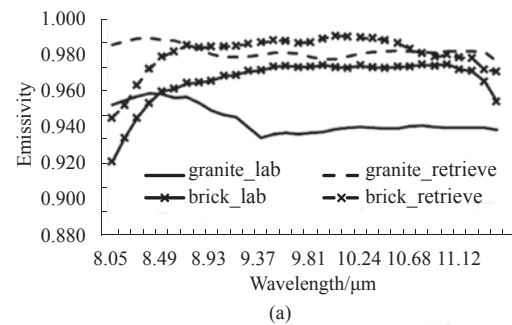


Fig. 7 Comparison of retrieved emissivity and lab-acquired emissivity “_lab” indicates the laboratory-measured data; “_measure” indicates the retrieved data

(a) Emissivity of granite, brick; (b) Emissivity of cement and roof

5.3 Application of urban surface temperature variation

Diurnal temperature range is representations of both daily variation amplitude and a simple thermal inertia model, and thus has very significant effect on urban microclimate. The data used in this part were two temperature images, dated at 5 a.m. and 2:30 p.m. Fig. 8 is the distribution of urban surface diurnal temperature range after image registration. The result shows that metal roof on summer has the maximum diurnal temperature range of above 30°C; the second are road, asphalt felt, and cement roof, whose diurnal temperature range vary from 12°C to 20°C; the third is vegetation, whose diurnal temperature range vary from 7°C to 10°C; the minimum are water and shadow, whose diurnal temperature range are less than 7°C. The reason for water is because of high heat capacity, high thermal inertia, and strong heat storage capacity and the temperature of shadow is lower for the same surface. So we can draw several conclusions from above analysis: (1) manmade building materials, especially metal materials are one of major factors of urban local heat island effect; water and urban landscaping can relieve urban heat island effect on a certain degree; (2) thermal inertia, as an inherent character, can be used as an effective index to distinguish and classify.

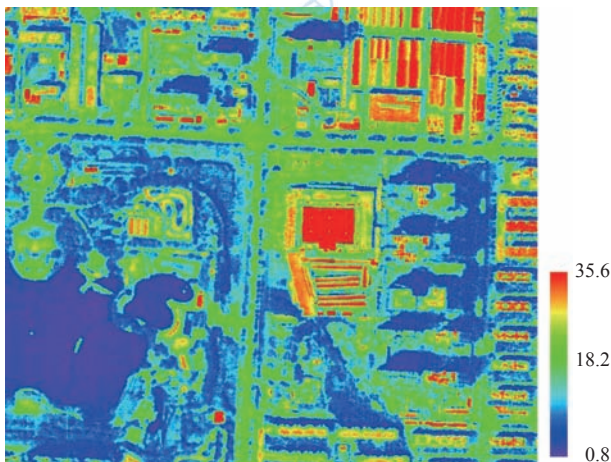


Fig. 8 Distribution of urban surface diurnal temperature range

6 CONCLUSION

To apply the algorithm of temperature and emissivity separation to thermal infrared airborne hyperspectral images, the new relationship between ϵ_{\min} and MMD was rebuilt. The research results show that for TASI data, there was very significant exponential relationship between ϵ_{\min} and MMD, and Eq. (10) shows that the relationship is close to a linear relation. The comparison between the retrieved emissivity of main building material and the laboratory measured emissivity demonstrates that the emissivity shapes acquired by the two methods are very similar. Considering the difference of atmosphere condition and field angle between laboratory and airborne experiment, the emissivity values of same surface type and wavelength setting are not same. The computation results of TASI broadband emissivity were in good agreement with field data

and the absolute difference was only 0.036, which shows that the reasonable accuracy.

This study demonstrates that the temperature deviation between retrieved and measured is within the scope. Because of the high space resolution of TASI data as mentioned above, there are many pure pixels in the images. So the evaluation of retrieval accuracy is more correct, and the result of validation is reliable. In a word, the TES algorithm could be applied to the study of thermal inertia, evapotranspiration and the urban energy balance. Finally, TES-derived temperature was used to diurnal temperature range. The results show that manmade building materials, especially metal materials are one of major factors of urban local heat island effect; water and urban landscaping can relieve urban heat island effect on a certain degree; thermal inertia, as an inherent character, can be used as an effective index to distinguish and classify.

REFERENCES

- Borel C C. 1998. Surface emissivity and temperature retrieval for a hyperspectral sensor. *Proceedings of the International Geoscience and Remote Sensing Symposium*, 1: 546–549
- Gillespie A R. 1985. Lithologic mapping of silicate rocks using TIMS//Kahle A B, Abbott E, eds. *The TIMS Data User's Workshop*, Pasadena: Jet Propulsion Laboratory Publication
- Gillespie A R, Matsunaga T, Rokugawa S, Cothren J S, Hook S and Kahle A B. 1998. A temperature and emissivity separation algorithm for advanced spaceborne thermal emission and reflection radiometer (ASTER) images. *IEEE Transactions Geoscience Remote Sensing*, 36(4): 1113–1126 DOI: 10.1109/36.700995
- Kahle A B, Madura D P and Soha J M. 1980. Middle infrared multispectral aircraft scanner data: analysis for geological applications. *Applied Optics*, 19(14): 2279–2290 DOI: 10.1364/AO.19.002279
- Kealy P S and Gabell A R. 1990. Estimation of emissivity and temperature using alpha coefficients. *Proceedings of the Second TIMS Workshop*. Pasadena: Jet Propulsion Laboratory, JPL Publication 90-55: 11–15
- Matsunaga T A. 1992. A temperature-emissivity separation method using an empirical relationship between the mean, the maximum and the minimum of the thermal infrared emissivity spectrum. *Journal of Remote Sensing Society of Japan*, 42: 83–106
- Schmugge T, Hook S J and Coll C. 1998. Recovering surface temperature and emissivity from thermal infrared multispectral data. *Remote Sensing of Environment*, 65(2): 121–131 DOI: 10.1016/S0034-4257(98)00023-6
- Sobrino J A, Jimenez-Munoz J C, Zarco-Tejada P J, Sepulcre-Cantó G and de Miguel E. 2006. Land surface temperature derived from airborne hyperspectral scanner thermal infrared data. *Remote Sensing of Environment*, 102(1-2): 99–115 DOI: 10.1016/j.rse.2006.02.001
- Yang H, Zhang L F, Fang J Y, Zhang X and Tong Q X. 2010. Algorithm Research of Building Materials Emissivity Extracting. IGARSS 2010, Honolulu HI: 3350-3353 DOI: 10.1109/IGARSS.2010.5650637
- Zhang RH. 2009. Models and field experiments for quantitative thermal infrared remote sensing. Beijing: Science Press: 97–100

TASI数据的温度与发射率分离算法

杨杭^{1,2}, 张立福¹, 张学文^{1,2}, 房丛卉³, 童庆禧¹

1. 遥感科学国家重点实验室 中国科学院遥感应用研究所, 北京 100101;
2. 中国科学院 研究生院, 北京 100039;
3. 中国地质大学(北京) 地球科学与资源学院, 北京 100083

摘要: 建立了适合于TASI的热红外高光谱发射率的经验关系, 以此修正了分离方法(TES)中的MMD模型, 在对温度和发射率进行精度评价的基础上, 将反演结果应用于城市地表温度的日较差分析。结果表明: (1)反演的温度与实测温度的平均绝对误差为1.8 K, 平均相对误差为0.59%; (2)地面实测宽波段发射率与反演发射率的平均差值为0.036, 差值的标准差为0.032; (3)同种地物的发射率曲线的反演结果与实验室测量发射率曲线的波形是一致的; (4)温度日较差分析结果是合理的。因此, 本文的反演精度能满足研究需求, 将该方法应用于TASI数据的温度与发射率的分离是可行的。

关键词: 热红外高光谱, 温度, 发射率, 日较差, TES

中图分类号: TP701 **文献标志码:** A

引用格式: 杨杭, 张立福, 张学文, 房丛卉, 童庆禧. 2011. TASI数据的温度与发射率分离算法. 遥感学报, 15(6): 1242-1254
Yang H, Zhang L F, Zhang X W, Fang C H and Tong Q X. 2011. Algorithm of emissivity spectrum and temperature separation based on TASI data. *Journal of Remote Sensing*, 15(6): 1242-1254

1 引言

成像光谱技术是人类获取和分析模拟环境数据的有力工具, 以往由于技术条件的限制, 热红外成像光谱技术的应用研究比较少。随着遥感技术的发展, 国内外越来越多的卫星携带有单个或几个热红外通道, 热红外数据逐渐为大家所重视。热红外数据反演得到地物的发射率光谱和温度对科学研究和实际应用具有极其重要的作用。地物发射率是地物的一个重要的特征物理量, 通过发射率研究可以进行地物识别和特征判读等; 温度数据是人类理解陆面过程的重要参数: 获取特定地表类型和生物物理组成的表面温度, 进而分析特定地表现象和过程的能量平衡特征(Sobrino 等, 2006)。因此温度和发射率的反演是热红外遥感研究中的核心问题。然而在其他参数精确确定的条件下, 温度和发射率的反演是一个 N 个方程和 $N+1$ 个未知数的欠定方程组, 必须假设或构建新的

方程使方程成为适定。但总的来讲, 不同研究方法因对发射率的假设不同而不同, 主要有参考通道法(Kahle 等, 1980)、发射率归一化法(Gillespie, 1985)、alpha剩余法(Kealy和Gabell, 1990)、MMD法(Matsunaga, 1992)、光谱平滑迭代算法(ISSTES)(Borel, 1998)和TES法(Gillespie 等, 1998)。其中ASTER提供的TES算法综合了NEM、RAT和MMD算法的优点。对ASTER数据模拟计算表明发射率误差在 ± 0.015 范围内(Yang 等, 2010), Schmutge 等(1998)将此方法用于荒漠草原的机载多光谱热红外数据, 结果误差为3 K。

以上研究还是以单波段和多光谱为主。随着硬件技术的发展, 热红外高光谱遥成为深入研究地物发射率和温度场创造了条件。光谱分辨率的提高, 使得地物发射谱的精细特征得以体现, 有助于形成相对更加稳定的约束条件, 提高反演精度。热红外航空成像光谱仪(Thermal Airborne Hyperspectral Imager, 简称TASI)是加拿大研制的先进的机载热红外高光谱

收稿日期: 2010-11-03; 修订日期: 2010-05-06

基金项目: 国家高技术研究发展计划(863计划)(编号: 2008AA121103, 2008AA121102); 国家自然科学基金(编号: 41072248)

第一作者简介: 杨杭(1979—), 男, 博士研究生, 现从事高光谱遥感理论及应用方面的研究。E-mail: yanghang1979@126.com。

通信作者简介: 张立福(1967—), 男, 研究员, 现从事高光谱遥感理论及应用方面的研究。E-mail: zhanglf@irsa.ac.cn。

设备。该设备在8—11.5 μm 范围内有32波段, 波段间隔为0.1095 μm , 半高宽为0.0548 μm , 总视场角为 40° 。图1为TASI在各波段传感器对辐亮度的灵敏度。本文旨在建立与TASI波段设置相适应的发射率经验模型, 将TES算法应用于TASI热红外高光谱数据, 在验证TES算法可靠性的同时研究分析地物温度分布和发射率性质, 进而探讨利用发射率谱识别地物的可能性。

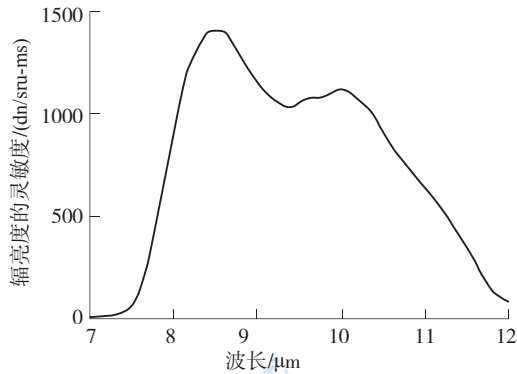


图1 TASI在各波段传感器对辐亮度的灵敏度

2 研究数据

飞行区域位于石家庄市, 介于 $38^\circ 0' 10''\text{N}$ — $38^\circ 6' 20''\text{N}$, $114^\circ 26' 34.01''\text{E}$ — $114^\circ 30' 0.01''\text{E}$, 南北长11.4 km, 东西宽5.03 km, 面积约 57.34 km^2 。2010-07-25—08-15在研究区进行热红外高光谱遥感实验, 获取了近红外/热红外的高光谱数据。TASI获取了早中晚3个时相的8—11.5 μm 范围内的32波段数据, 每个时相有0.5 km和1 km两个航高, 飞行的详细时间安排见表1, 航拍时采用垂直对地观测。图2为选取的研究区域的彩色图像。

表1 航空试验飞行时间和飞行高度

飞行时间	飞行高度/km
2010-07-25中午	0.5
2010-07-25傍晚	0.5
2010-07-27傍晚	1.0
2010-07-29早上	0.5
2010-08-07早上	1.0
2010-08-15中午	1.0

飞行的同时还进行了地面典型地物的温度和发射率测量。其中温度测量时, 地面同步实验与飞机过顶时间前后相差不超过5 min, 每个地面样本点均匀读取温度数据20—30个, 取其均值作为实测值, 同时记录该点的经纬度坐标。所用仪器为多光谱热红外地面辐射计(CE312)和MINOLTA/LAND红外测温仪, 这两种仪器的精度均在0.1 K左右。主要测量地物为路面(水泥和沥青)、农作物(玉米、地瓜和花生等)、建筑屋顶、水体和广场等。这些同步测量数据将用于温度和反射率反演以及反演结果的精度评价。



图2 选取的研究区域

3 数据处理

3.1 数据定标

(1) TASI数据的辐射定标

为了获取有用地物的目标辐射信号, 在测量地物目标的辐亮度之前需要对设备的每个波段进行辐射定标, 也就是将热红外成像光谱仪输出电压的数字值(DN值)转换为光谱辐射亮度值。TASI的辐射定标方法是在假定仪器响应函数为线性的基础上, 通过测量两个已知温度和发射率的标准黑体来实现的。假定TASI光谱仪输出DN与输入的辐射亮度L是线性的, 则通过式(1)就可以逐波段逐像元的进行辐射定标。

$$L = c_1 \times DN + c_2 \quad (1)$$

式中, c_1 和 c_2 分别是仪器的响应函数的增益和偏置, 该过程是由TASI自带软件系统完成的。

(2) 红外测温仪的定标

与普通温度计相比, 红外测温仪器稳定性弱, 容

易衰减,因此每次试验前后各进行一次定标试验。仪器的定标采用盆装纯净水代替黑体。定标需要用冷水和热水,其中冷水选用常温水,热水温度一般在45℃以上,用水温计测量水温。定标时,水体须充满仪器视场,待水体温度稳定并且均匀时再进行测量,并记录下水温。

定标时,把水温计测量的温度作为真实温度,水温计测得冷水的温度记为 $T_{1,true}$,红外仪测得温度记为 $T_{1,R}$;水温计测得热水温度记为 $T_{2,true}$,红外仪测得温度记为 $T_{2,R}$ 。辐射温度和真实温度之间存在线性关系:

$$T_{true} = k_1 \times T_R + k_2 \quad (2)$$

将上面实测的 $T_{1,true}$ 、 $T_{1,R}$ 和 $T_{2,true}$ 、 $T_{2,R}$ 分别代入式(2)可求得系数 k_1 和 k_2 ,从而实现对每个红外温度值进行定标。

3.2 大气校正

大气校正实现了从传感器辐亮度到地面辐亮度的转换。假设地表为朗伯体,并结合Kirchhoff定律,机载红外高光谱传感器接收到的地表辐亮度可以用下式来表达:

$$L_i = \tau_i \varepsilon_i B_i(T_s) + \tau_i (1 - \varepsilon_i) L_{atm\downarrow,i} + L_{atm\uparrow,i} \quad (3)$$

式中, L_i 为传感器接收到的第 i 波段的辐射亮度值; ε_i 为第 i 波段的比辐射率; $B_i(T_s)$ 为黑体在目标物辐射温度 T_s 下的发射辐射; τ_i 为第 i 波段的大气透过率; $L_{atm\uparrow,i}$ 为大气上行辐射; $L_{atm\downarrow,i}$ 为大气下行辐射。

针对本次试验区域,采用MODTRAN软件获取了与TASI波段设置相一致的大气上(下)行辐射和透过率。其中主要参数设置为:

(1) 大气资料的输入

选用中纬度夏季大气模式,大气路径设置为倾斜;大气水汽含量采用气象观测数据。二氧化碳含量设置为380 ppmv,多次散射模型选用离散纵坐标法软件包中的8流近似法。大气第一边界层的温度采用试验场同步观测的近地面大气温度。

(2) 气溶胶资料的输入

选用的气溶胶模式为城市气溶胶,能见度为5 km,季节模式选用春夏季,风速为同步测量值,选择天气为无云和雨。

图3为用MODTRAN反演的与TASI波段设置相一致的大气上(下)行辐射,图4为大气透过率曲线。

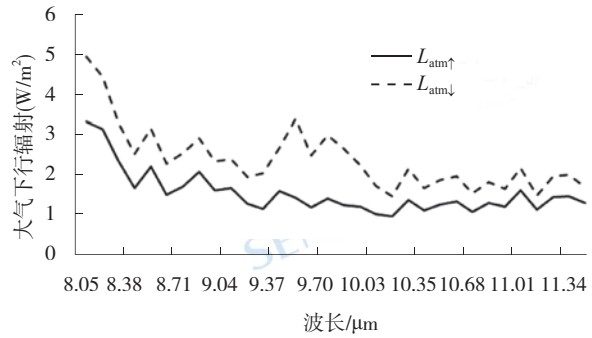


图3 用MODTRAN得到的与TASI波段相对应的大气上(下)行辐射

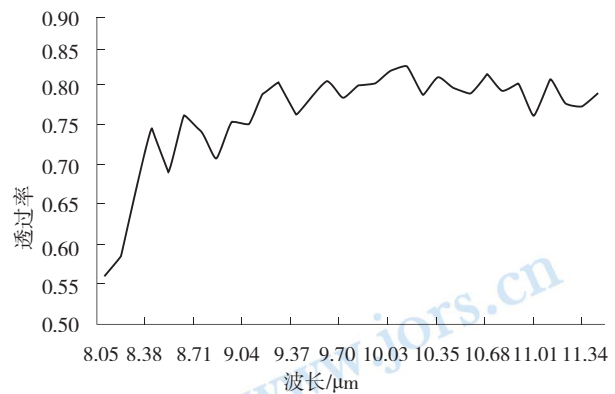


图4 用MODTRAN模拟得到的与TASI波段相对应的大气透过率

因此在获取目标温度最佳估计值的前提下,目标发射率可以由下式计算:

$$\varepsilon_i = \frac{L_{gi} - L_{atm\downarrow,i}}{B_i(T_s) - L_{atm\downarrow,i}} \quad (4)$$

式中, $L_{gi} = (L_i - L_{atm\uparrow,i}) / \tau_i$ 。

4 温度与发射率的反演

4.1 温度与发射率反演(TES)算法

Gillespie等人(1998)针对Aster数据研发了一种新的温度、发射率分离算法,它综合了NEM、Ratio和MMD这3个基本模块。

NEM模块(normalized emissivity method, 标准化发射率):先假定对 N 个波段的发射率都赋予一个初始的定值 $\varepsilon_0=0.97$,通过多次迭代以尽可能地消除天空辐射的影响,进而得到一个初始的地表温度的估计值 T_s^0 。

Ratio模块:该模块通过式(5)得出发射率的相对谱形,保持了在迭代过程中发射率光谱形状,是该模

块的重要优点。

$$\beta_i = \frac{\varepsilon_i}{\bar{\varepsilon}} = \frac{L_i / B_i(T_s^0)}{\left(\frac{1}{N} \sum_{i=1}^N L_i\right) / \left(\frac{1}{N} \sum_{i=1}^N B_i(T_s^0)\right)} \quad (5)$$

式中, L_i 为大气纠正后的第*i*波段的辐射亮度, T_s^0 为NEM模块计算的初始温度, ε_i 为第*i*波段的发射率, $\bar{\varepsilon}$ 为平均发射率, N 为波段数, 对TASI数据, $N=32$ 。

MMD模块: 利用最小发射率 ε_{\min} 与 β 谱的最大值与最小值之差(即 $MMD = \max(\beta) - \min(\beta)$)的经验关系(式(6)), 求出发射率的最小值。

$$\varepsilon_{\min} = a - b \times MMD^c \quad (6)$$

式中, 系数*a*、*b*、*c*是基于光谱库数据拟合得出的, 应用于不同的传感器数据时, 这些系数的值是不同的, 因此应首先考虑建立与TASI波段设置相适应的发射率经验关系, 以提高反演精度。

4.2 地表宽波段(8—12 μm)发射率的测量

采用张仁华(2009)提出的便携式比辐射率测定仪, 测量不同地表类型的宽波段比辐射率。简单表述如下:

测量原理与黑体筒封闭法相同, 在冷热两次环境辐照度下有两个方程:

$$M'_{s1} = \varepsilon_B M'_{B1} + (1 - \varepsilon_B) M'_{E1} \quad (7)$$

$$M'_{s2} = \varepsilon_B M'_{B2} + (1 - \varepsilon_B) M'_{E2} \quad (8)$$

式中, M'_{s1} 为冷环境下目标物的出辐射度, M'_{s2} 为热环境下目标物的出辐射度, M'_{B1} 为冷环境下目标物的辐亮度, M'_{B2} 为热环境下目标物的辐亮度, M'_{E1} 为大气下行辐射照度, M'_{E2} 为腔体内热辐射照度, ε_B 为目标物的发射率。其中, M'_{s1} 、 M'_{s2} 、 M'_{E1} 和 M'_{E2} 可以直接测量得出, 而方程中两次测量的目标辐射亮度相等, 即 $M'_{B1} = M'_{B2}$, 故两个方程只有两个未知数 M_B 和 ε_B , 应用Stefan-Boltzman定律可求出发射率, 计算公式为:

$$\varepsilon = 1 - \frac{M'_{s1} - M'_{s2}}{M'_{E1} - M'_{E2}} = 1 - \frac{T_{s1}^4 - T_{s2}^4}{T_{E1}^4 - T_{E2}^4} \quad (9)$$

式中, T_{s1} 、 T_{s2} 、 T_{E1} 和 T_{E2} 分别为辐亮度为 M'_{s1} 、 M'_{s2} 、 M'_{E1} 和 M'_{E2} 的黑体温度。

4.3 TES发射率经验关系的建立

运用ASTER和MODIS波谱库中提供的274条光谱

曲线, 将它们统一转化成发射率曲线, 地物类型包括水体、植被、土壤、矿物、建筑材料以及部分人工地物, 基于这些数据建立与TASI相一致的经验关系, 步骤如下:

(1)将这些数据重采样成与TASI波段设置相一致的发射率曲线。

(2)运用式(5)计算每种地物各波段发射率与该曲线均值的比值。

(3)计算 $MMD = \max(\beta_i) - \min(\beta_i)$ ($i=1-32$)。

(4)经验关系的建立: 经拟合得到如下显著指数关系(图5):

$$\varepsilon_{\min} = 0.9924 - 0.9174 \times MMD^{0.9723} \quad (10)$$

$(r^2 = 0.988, SD = 0.0156)$

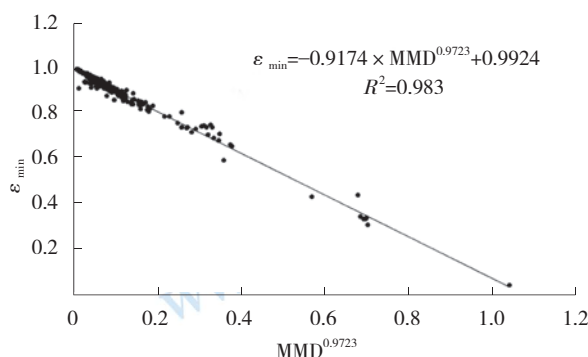
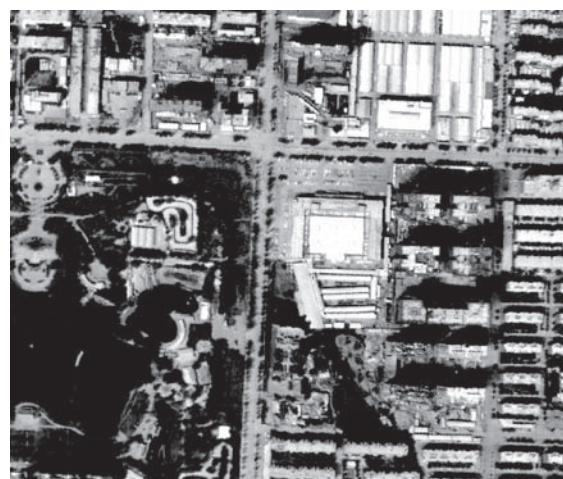


图5 ε_{\min} 与MMD的指数关系

将建立的新发射率经验关系替代TES算法中的发射率模型, 即可对TASI数据应用于TES算法以获取发射率和温度信息。图6为反演的2010-08-15中午获取的TASI影像温度图与发射率图。



297.9 315.2 332.5
(a)

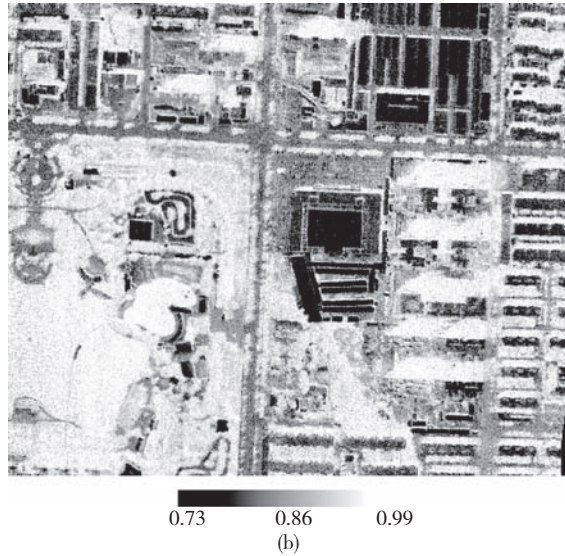


图6 TES方法反演结果
(a) 温度; (b) 发射率

5 反演结果分析

对于地表温度反演算法的精度评价通常采用两种方法: 大气模拟数据法和地面实测数据法。本文采用实测数据法进行结果分析, 反演的结果精度分析主要从温度和发射率两个方面进行分析。

5.1 温度反演精度分析

在进行温度精度分析前, 应首先将红外测温仪测量温度进行黑体定标。由于TASI传感器在航高为0.5 km时机下点空间分辨率为0.59 m, 1 km时机下点的空间分辨率为1.19 m。因此根据地面同步试验中测点的经纬度坐标找到对应的机载热红外数据反演的温度值, 并与地面同步实验获取的温度值比较, 结果统计见表2。

表2 温度反演结果与实测结果比较

地物类型	实测值/K	反演值/K	反演误差/K	相对误差/%
柏林小区屋顶	302.6	306.4	3.8	1.26
联强小区屋顶	304.4	304.7	0.3	0.10
水泥广场	305.0	306.3	1.3	0.42
水泥路面1	316.2	313.2	3.1	0.97
水泥路面2	304.0	306.4	2.5	0.81
农田内草地	304.0	303.0	1.0	0.34
玉米	295.7	293.8	2.0	0.66
公园内草地	295.8	295.0	0.9	0.29
公园内花岗岩路面	297.1	296.8	0.3	0.11
公园内水体	299.3	298.5	0.9	0.29

续表

地物类型	实测值/K	反演值/K	反演误差/K	相对误差/%
河水温度	299.2	300.7	1.6	0.52
黑布	311.2	307.3	3.9	1.25
白布	307.9	305.8	2.1	0.68
温度偏差均值			1.8	0.59
偏差均值的标准差			1.2	0.39

由表2可知, 反演结果与实测数据相比误差从0.3 K到3.9 K, 平均绝对误差为1.8 K, 平均相对误差为0.59%。其中联强小区屋顶、公园内花岗岩路面的温度反演精度最高, 误差为0.3 K, 而柏林小区屋顶的温度反演误差为3.8 K, 这是因为柏林小区屋顶上布满了太阳能热水器, 严重影响了反演精度, 而联强小区屋顶比较均一。同样是水泥, 广场的反演温度偏差为1.3 K, 路面的反演温度偏差为2.5 K和3.1 K, 这是因为广场视野相对比较宽阔, 而道路受城市建筑、绿化乔木等的影响严重。公园水体的反演温度偏差为0.9 K, 而河水的反演温度偏差为1.6 K, 这可能是公园内水体是静止的而河水温度受其流动性的影响造成的。黑布的温度反演误差较大, 为3.9 K, 可能是由于该黑布铺在比较空旷的倾斜河岸上, 斜坡角度对反演误差造成了较大的影响。

5.2 发射率反演精度分析

为了分析地表发射率反演精度, 将TASI发射率转换成宽波段发射率与地面实测宽波段发射率进行对比分析(表3), 可知地表发射率的反演值与实测值的平均差值为0.036, 差值标准差为0.032。

表3 地表发射率反演值和实测值对比

地物类型	实测值	反演值	差值
黑色油毡细粉砂屋顶	0.948	0.953	0.005
绿色油毡细粉砂屋顶	0.928	0.882	0.046
黑色油毡屋顶	0.953	0.904	0.049
红色塑胶跑道	0.998	0.917	0.081
炭渣跑道	0.977	0.930	0.047
沥青路面	0.912	0.910	0.002
白色水泥路面	0.910	0.917	0.007
裸土	0.959	0.957	0.002
菜地	0.981	0.951	0.030
假草坪	0.976	0.891	0.086
均值			0.036
差值的标准差			0.032

TASI的优势更在于其为高光谱, 因此有必要进一步分析其反演的发射率谱线与实际发射率的差异。

图7结果显示, 主要城市建筑材料, 如花岗岩(granite)、砖(brick)、水泥(cement)以及屋顶(roof)材料的反射率反演结果虽然与实验室测量结果的绝对值并不相同, 甚至有的相差比较大, 但是同种地物的两种结果之间的波形是一致的。这是由于实验室测得的样本表面发射率与像元尺度发射率有着巨大差异, 且机载数据的大气效应不可能完全消除, 另外实验室测量对表面粗糙度极为敏感, 因此反演发射率与实验室测量发射率只能进行形状比较。

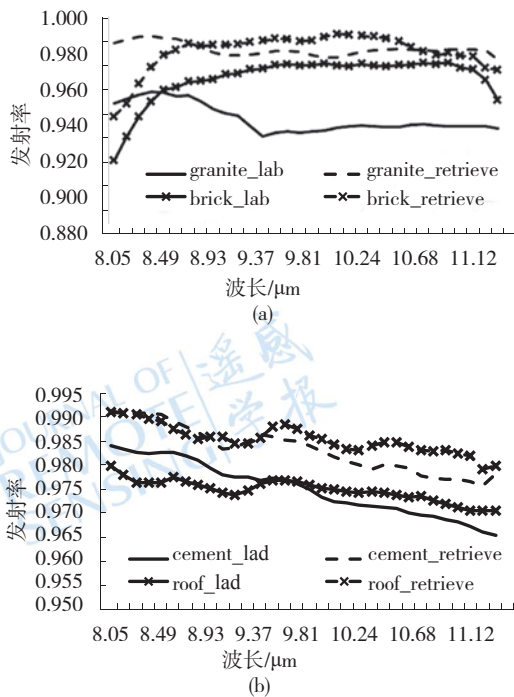


图7 反演所得发射率与实验室测得发射率比较
“_lab”为实验室测得数据, “_retrieve”为反演结果
(a) 花岗岩和砖的发射率; (b) 水泥和屋顶的发射率

5.3 温度变化监测应用

地物表面温度的日较差反映了地表温度的日变化振幅的大小, 是一种最简单的热惯量模型, 地表温度的日较差对城市小气候的影响极其显著。选取早上5点的温度分布图像和下午两点半的温度图像, 经过配准后计算其温差(图8)。

图8结果表明, 夏季金属屋顶的日较差最大, 最大可达 30°C 以上; 其次是道路、油毡与水泥屋顶, 其日较差一般在 12°C — 20°C ; 再次是植被, 其日较差一般为 7°C — 10°C ; 水体和阴影的日较差最低, 小于 7°C , 水体日较差小是因为水体的比热大, 热惯量大, 储热能力强, 阴影温差小是因为阴影对应的温度

低于同类地表的光照面温度。

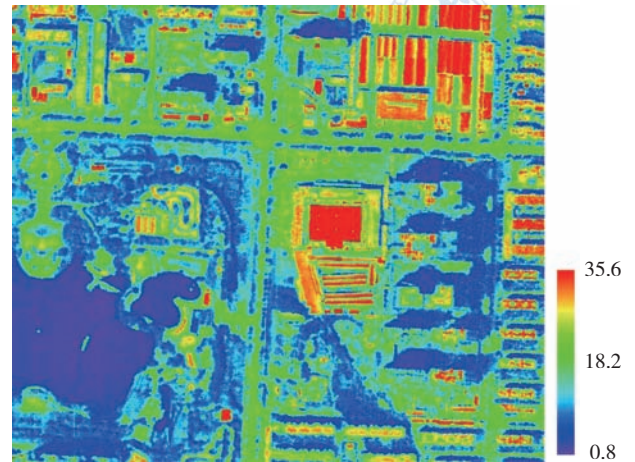


图8 城市地表日较差分布图

6 结论

将温度与发射率分离算法(TES)用于航空热红外高光谱图像的温度与反射率反演, 并重新构建了 ϵ_{\min} 与MMD之间的关系。研究表明: 对于TASI热红外高光谱数据, ϵ_{\min} 最小值与MMD呈显著指数关系, 但是从该关系式看出, 二者之间的关系已经非常接近线性关系。将反演主要建筑材料的发射率结果与实验室测量数据进行比较, 结果发现: 反演结果与实验室测量波谱在波形上很相似。考虑到实验室测量与航空影像获取的大气条件及其视场角等的差异, 它们之间的发射率数值并不相等。将TASI反演的发射率转化成宽波段发射率并与野外实际测量发射率进行对比, 平均差值仅为0.036, 具有较高的精度。

结果还发现, 反演的温度与地面同步测量的红外温度的偏差在合理范围内。由于TASI的空间分辨率较高, 航高为1 km时机下点空间分辨率为1.19 m, 航高为0.5 km时机下点空间分辨率为0.59 m。在这样的空间分辨率下, 影像上存在大量的纯像元, 因此温度的反演结果是比较准确的, 且真实性检验的结果可靠, 可以将其应用于热惯量、蒸散模型以及城市能量平衡的研究中。本研究将温度反演结果应用于城市地表温度的日较差模型, 分析结果表明: (1)人工建筑材料, 尤其是金属材料是造成城市局地热岛效应的主要因素之一, 城市内水体和绿化能从一定程度上缓解城市热岛效应; (2)作为地物固有特性的热惯量可以作为地物识别和分类的一个有效指标。

REFERENCES

- Borel C C. 1998. Surface emissivity and temperature retrieval for a hyperspectral sensor. *Proceedings of the International Geoscience and Remote Sensing Symposium*, **1**: 546–549
- Gillespie A R. 1985. Lithologic mapping of silicate rocks using TIMS//Kahle A B, Abbott E, eds. *The TIMS Data User's Workshop*, Pasadena: Jet Propulsion Laboratory Publication
- Gillespie A R, Matsunaga T, Rokugawa S, Cothorn J S, Hook S and Kahle A B. 1998. A temperature and emissivity separation algorithm for advanced spaceborne thermal emission and reflection radiometer (ASTER) images. *IEEE Transactions Geoscience Remote Sensing*, **36**(4): 1113–1126 DOI: 10.1109/36.700995
- Kahle A B, Madura D P and Soha J M. 1980. Middle infrared multispectral aircraft scanner data: analysis for geological applications. *Applied Optics*, **19**(14): 2279–2290 DOI: 10.1364/AO.19.002279
- Kealy P S and Gabell A R. 1990. Estimation of emissivity and temperature using alpha coefficients. *Proceedings of the Second TIMS Workshop*. Pasadena: Jet Propulsion Laboratory, JPL Publication 90-55: 11–15
- Matsunaga T A. 1992. A temperature-emissivity separation method using an empirical relationship between the mean, the maximum and the minimum of the thermal infrared emissivity spectrum. *Journal of Remote Sensing Society of Japan*, **42**: 83–106
- Schmugge T, Hook S J and Coll C. 1998. Recovering surface temperature and emissivity from thermal infrared multispectral data. *Remote Sensing of Environment*, **65**(2): 121–131 DOI: 10.1016/S0034-4257(98)00023-6
- Sobrino J A, Jimenez-Munoz J C, Zarco-Tejada P J, Sepulcre-Cantó G and de Miguel E. 2006. Land surface temperature derived from airborne hyperspectral scanner thermal infrared data. *Remote Sensing of Environment*, **102**(1-2): 99–115 DOI: 10.1016/j.rse.2006.02.001
- Yang H, Zhang L F, Fang J Y, Zhang X and Tong Q X. 2010. Algorithm Research of Building Materials Emissivity Extracting. IGARSS 2010, Honolulu HI: 3350-3353 DOI: 10.1109/IGARSS.2010.5650637
- Zhang R H. 2009. *Models and field experiments for quantitative thermal infrared remote sensing*. Beijing: Science Press: 97–100

附中文参考文献

- 张仁华. 2009. 定量热红外遥感模型及地面实验基础. 北京: 科学出版社: 97–100